

EFFECT OF MOLYBDENUM ON THE PRECIPITATION BEHAVIOR IN TITANIUM MICROALLOYED HSLA STEELS PART I – PRECIPITATION IN AUSTENITE

Sun Xinjun, Wang Zhenqiang, Yong Qilong and Dong Han

Central Iron and Steel Research Institute (CISRI), Beijing, China

Keywords: Precipitation, HSLA Steel, TiC, Molybdenum, HRTEM, Stress Relaxation, Titanium, Phase Transformation, Microhardness, Interphase Precipitation

Abstract

The carbide precipitation behavior in austenite of a 0.04%C-0.10%Ti-0.21%Mo microalloyed steel was investigated by the stress relaxation test method and transmission electron microscopy. Results showed that the precipitation-time-temperature diagram for carbide precipitation exhibited a typical “C” curve, the nose of which was located at about 925 °C. The carbide was identified as a (Ti,Mo)C particle with a NaCl-type crystal structure that contained a certain amount of Mo. As compared with TiC particles in a Ti steel, (Ti,Mo)C particles in a Ti-Mo steel exhibit a superior coarsening resistance during the coarsening stage. The fraction of Mo in the (Ti,Mo)C particles decreases with longer isothermal holding time or particle growth, indicating that the high level of replacement of Ti by Mo in the TiC lattice is in a “metastable” state with respect to the equilibrium precipitation of (Ti,Mo)C in austenite.

Introduction

In order to reduce fuel consumption, weight and improve product quality in automobiles, advanced high strength low alloy steels have been investigated and developed [1-5]. In recent work performed at JFE Steel Corporation [1], tensile strengths of 780 MPa with excellent stretch flange formability have been obtained in Ti-Mo bearing, low C sheet steels, by producing a microstructure that only consists of ferrite and nanometer-sized carbides. The contribution to the yield strength from precipitation strengthening was estimated to be approximately 300 MPa, which was attributed to nanometer-sized (Ti,Mo)C precipitates that were formed at the austenite-ferrite interfaces during transformation. Subsequently, many researchers, eg. Yen et al. [6,7] and Jang et al. [8], using high resolution transmission electron microscopy (HRTEM) and/or first-principles calculations, systematically studied these nanometer-sized (Ti,Mo) carbides, including their crystal structure, orientation relationship with respect to the ferrite and the role of Mo in relation to coarsening resistance. They found that the (Ti,Mo) carbides possessed a NaCl-type crystal structure with a lattice parameter of ~0.430 nm, and adopted a Baker–Nutting orientation relationship with respect to ferrite. More importantly, these (Ti,Mo)C particles had an excellent thermal stability due to the decrease in the interfacial energy with the ferrite matrix caused by the partial replacement of Ti by Mo in the TiC lattice [8].

Another significant contribution to the yield strength, up to ~280 MPa, in Ti-Mo bearing steels produced by JFE Steel Corporation, came from grain refinement strengthening. The average ferrite grain size of a Ti-Mo microalloyed steel in their work was measured as only 3.1 μm . It is well established that the precipitation of microalloying elements in austenite plays an important role in controlling the final microstructure. In the case of conventional controlled rolling, roughing deformation is succeeded by a fast cooling phase and finishing passes are carried out at temperatures where the austenite remains unrecrystallized. Microalloying elements such as Ti, which remain in solution during roughing deformation, start precipitating following the finish rolling at low temperatures. These fine precipitates, such as TiC, play an effective role in retarding recovery and recrystallization of deformed austenite, thus helping to retain the accumulated strain and deformed structure of the austenite grains. This in turn leads to a high ferrite nucleation rate during subsequent $\gamma \rightarrow \alpha$ phase transformation, thus favoring the refinement of the final microstructure and the improvement of the product properties [9-11]. In our previous reports and some other references [12-14], the carbonitride precipitation behavior after austenite deformation in Ti microalloyed steels was systematically studied using various hot deformation methods, including high temperature flow curves, stress relaxation tests and the two stage interrupted method. The precipitation kinetics curves, ie. precipitation-time-temperature (PTT) diagrams, were determined by different methods and all exhibited a typical “C” shape curve. In addition, the precipitates were identified by TEM as TiC or Ti(C,N) particles with a NaCl-type crystal structure, and they were considered to be nucleated on dislocations and dislocation sub-structures in hot worked austenite. The growth of the precipitates approximately followed a parabolic law during the growth stage, and then entered into a coarsening stage with a time exponent of ~0.1 [12,13]. However, as compared to carbonitride precipitation in Ti microalloyed steel and other complex carbonitride precipitation in Ti-V and Nb-V microalloyed steels [15], carbide precipitation in Ti-Mo microalloyed steels during hot working in austenite has not been extensively investigated, although many studies on carbide precipitation in ferrite or during $\gamma \rightarrow \alpha$ phase transformation of Ti-Mo microalloyed steel have been conducted by many researchers as mentioned above. Therefore, based on the importance of microalloying element precipitation in hot worked austenite, the purpose of this work was to investigate, using systematic stress relaxation experiments, high resolution electron microscopy and thermodynamics calculation, the kinetics of carbide precipitation in austenite and the crystal structure, nucleation, growth, coarsening and compositional evolution of precipitates in a Ti-Mo microalloyed steel. In addition, the coarsening resistance of carbides in a Ti-Mo microalloyed steel is discussed by comparing with that in a Ti microalloyed steel.

Experimental

The chemical compositions of the investigated steels are given in Table I. The Ti-Mo microalloyed steel has a base composition of 0.04%C-0.10%Ti-0.21%Mo wt.%. A Ti microalloyed steel with the composition of 0.05%C-0.10%Ti wt.% was used here as a reference steel to study the role of Mo in terms of the size evolution of precipitates. The two experimental steels were prepared by vacuum melting, and then hot forged to 20 mm diameter rods. After homogenization in the austenite phase field for 300 minutes at 1200 °C, followed by water quenching, the cylindrical specimens, with 8 mm diameter and 12 mm length for hot compression tests, were cut from the center of the as-homogenized rods using electrical discharge machining. In order to study the precipitation kinetics in the Ti-Mo microalloyed steel,

stress relaxation tests [12] were performed using a Gleeble 1500D simulator. The specimens were first preheated at 1150 °C for 3 minutes to dissolve all carbides except a small amount of TiN particles, and then cooled to a deformation temperature in the range of 875 °C to 975 °C, which was chosen to be in the austenitic phase field due to the phase transformation critical temperature (A_{e3}) being 855 °C as calculated by Thermo-calc with database TCFE6. At this temperature, the specimen was compressively deformed by a 20% reduction along its main axis at a strain rate of 1.0 s^{-1} . The reduction of 20% is very close to the value attained in one industrial rolling pass. Relaxation of the applied compressive stress was then monitored as a function of time up to 50 minutes, before the specimen was cooled by water quenching. In order to study the size evolution of precipitates in Ti-Mo and Ti microalloyed steels, stress relaxation tests with shorter holding times were also conducted. Extraction replica methods [12,13] were used to study the precipitates in the investigated specimens. Each specimen was sectioned perpendicular to the deformation axis, polished, and then etched in 4% nital for about 1 minute. A carbon layer about 20 nm in thickness was deposited on the treated surface using an evaporator. The carbon coated surfaces of the specimens were then scribed using a knife to produce squares about 3×3 mm in size. The replicas were released in the same etching solution, and then analyzed in a field emission gun scanning transmission electron microscope (Tecnai F20). The sizes of the precipitates were measured by a quantitative image analyzer, and the results were obtained by averaging at least two hundred measurements. Chemical analyses of the precipitates were determined using nano-beam energy-dispersive spectroscopy (EDS). At least ten precipitates, formed during stress relaxation, were analyzed for each specimen by TEM/EDS to examine the compositional evolution of precipitates in the Ti-Mo microalloyed steel with isothermal holding time. Each EDS data point was obtained from the whole area of each individual precipitate projection as viewed in TEM mode. In addition, the equilibrium chemical composition of the precipitate, in the Ti-Mo microalloyed steel, over the temperature range 500-1000 °C was calculated by Thermo-calc with the database TCFE6.

Table I. Chemical Compositions of the Investigated Steels

Steel		C	Mn	Si	Ti	Mo	N
Ti-Mo	wt. %	0.04	1.51	0.20	0.10	0.21	0.002
	at. %	0.19	1.54	0.40	0.12	0.12	0.008
Ti	wt. %	0.05	1.47	0.12	0.10	-	0.002
	at. %	0.23	1.50	0.24	0.12	-	0.008

Results and Discussion

Stress Relaxation Curve and Precipitation-time-temperature Diagram of Ti-Mo Microalloyed Steel

The stress relaxation curves of the Ti-Mo microalloyed steel at different temperatures are shown in Figure 1. As stated earlier, all the deformation temperatures were chosen to be in the austenitic phase field. Liu and Jonas [12] suggested that strain induced precipitation in deformed austenite occurs mostly on the dislocations and sub-boundaries developed by deformation, which implies that austenite grain size will not be a dominant factor in influencing the precipitation kinetics. In Figure 1, the stress relaxation curves at 950 °C and below exhibit an initial linear stress drop (with respect to log time), which corresponds to a static recrystallization process [15]. After the linear stress drop process, a relaxation stress plateau appears in these curves, indicating the onset of strain induced precipitation, which halts the progress of recrystallization. The relative dominance of these two processes depends on the relative magnitudes of F_R (driving force for recrystallization front migration) and F_{Pin} (retarding force due to pinning of dislocations by precipitated particles). If $F_R < F_{Pin}$, the interfaces will be completely arrested. Initially the driving force for recrystallization is greater owing to a large amount of stored energy in the form of a heavily dislocated matrix. Recrystallization and precipitation are competing processes and progress of recrystallization can be halted by the drag exerted on the migrating grain boundaries by the presence of solute Ti and Mo or by Zener pinning exerted by the strain induced precipitates which preferentially nucleate on dislocations. The precipitates grow faster due to pipe diffusion along dislocations and once the precipitates coarsen sufficiently, recrystallization again takes over resulting in the fall in stress as indicated in the relaxation curves. Liu and Jonas [12] also suggested that the stress vs log (time) relationship under this condition can be described as follows:

$$\sigma = \sigma_0 - \alpha \log(1 + \beta t) + \Delta\sigma \quad (1)$$

where σ is the relaxation stress, σ_0 is the initial stress, t is the holding time after deformation in seconds, α and β are experimental constants and $\Delta\sigma$ is the stress increment due to precipitation. For sufficiently long times, $\beta t \gg 1$, Equation (1) becomes:

$$\sigma = A - \alpha \log t + \Delta\sigma \quad (2)$$

Here, $A = \sigma_0 - \alpha \log \beta$. According to Equation (2), $\Delta\sigma$ equals ~ 0 during the initial linear stress drop stage. As relaxation proceeds, $\Delta\sigma$ increases gradually and finally reaches the maximum value at a certain time which is marked by arrow (P_f) in Figure 1. The maximum value of $\Delta\sigma$ is also a function of testing temperature and it decreases with increasing temperature as shown in Figure 2. That is because of the decrease of the volume fraction of precipitates and the increase of precipitate size with increasing isothermal temperature [9,10,13]. The stress relaxation curve at 975 °C does not show a relaxation plateau just after a linear-drop stage. Instead, a fast drop in stress value appears after a linear-drop stage, which indicates the occurrence of static recrystallization, as marked by SRX in Figure 1. It is known that the recrystallization progress results in a rapid drop in the density of structural defects such as dislocations in the deformed

austenite matrix. Since these defects are the nucleation sites for strain induced precipitates [16], their rapid disappearance at the high temperature of 975 °C is expected to hinder the precipitation process. The stress plateau after the fast-drop stage could result from static recovery of austenite.

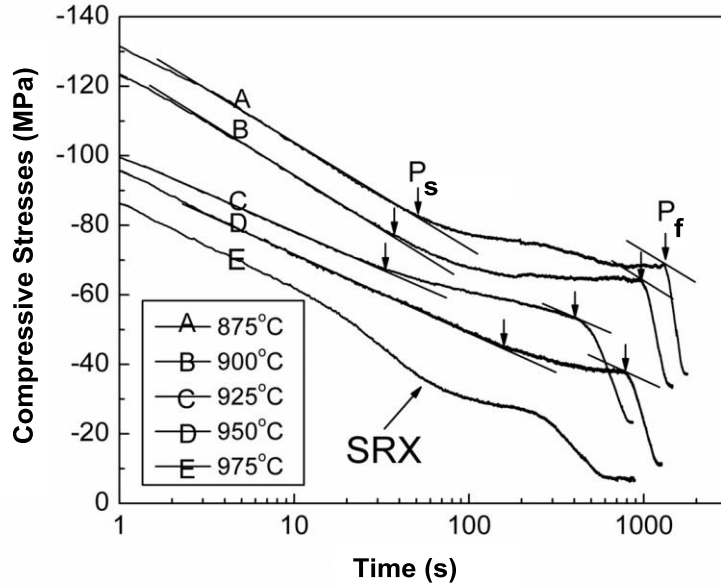


Figure 1. Stress relaxation curves of the Ti-Mo microalloyed steel at different temperatures. SRX denotes fast static recrystallization. P_s and P_f represent the start and finish times of the plateau, respectively.

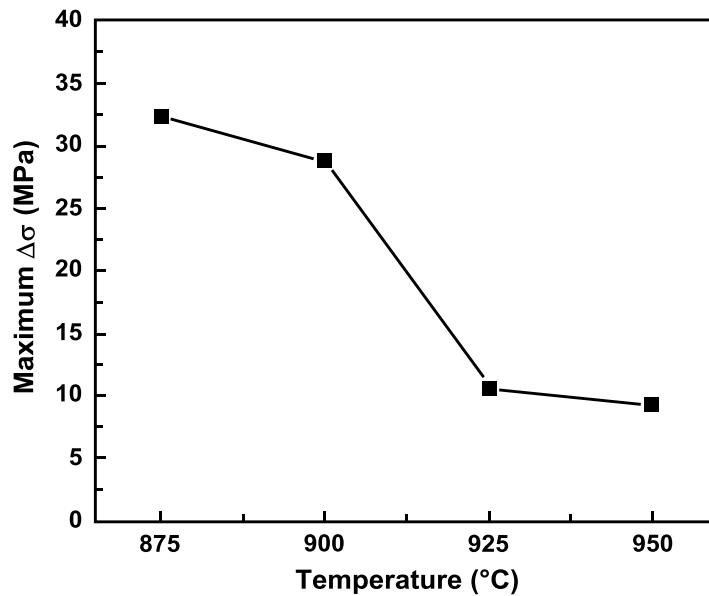


Figure 2. Maximum $\Delta\sigma$ as a function of testing temperature.

According to previous workers [12], the start and finish times of the plateau on the stress relaxation curves, which are marked by arrows in Figure 1, are defined as the onset (P_s) and end (P_f) times respectively of the precipitation process induced by strain. The P_s point indicates the onset of the precipitation, and the P_f point represents the time at which the precipitation hardening reaches the maximum, i.e. $\Delta\sigma$ reaches its maximum value. It should be noted that the P_f point does not denote the volume fraction of precipitates reaching an equilibrium value, but possibly represents the transition of the mechanism of particle growth [16]. The precipitation-time-temperature (PTT) diagram for carbide precipitation in the Ti-Mo microalloyed steel was successfully obtained as shown in Figure 3. The PTT diagram exhibits a typical “C” shape; its nose, which corresponds to the minimum incubation time for precipitation, is located at about 925 °C. This temperature is very close to that of TiC precipitation reported in our previous work on a Ti microalloyed steel with a similar chemical composition, but without a Mo addition [13]. In addition, the start time shown in the PTT diagram is within 50 seconds in the temperature range of 875-925 °C, but exceeds 150 seconds at 950 °C.

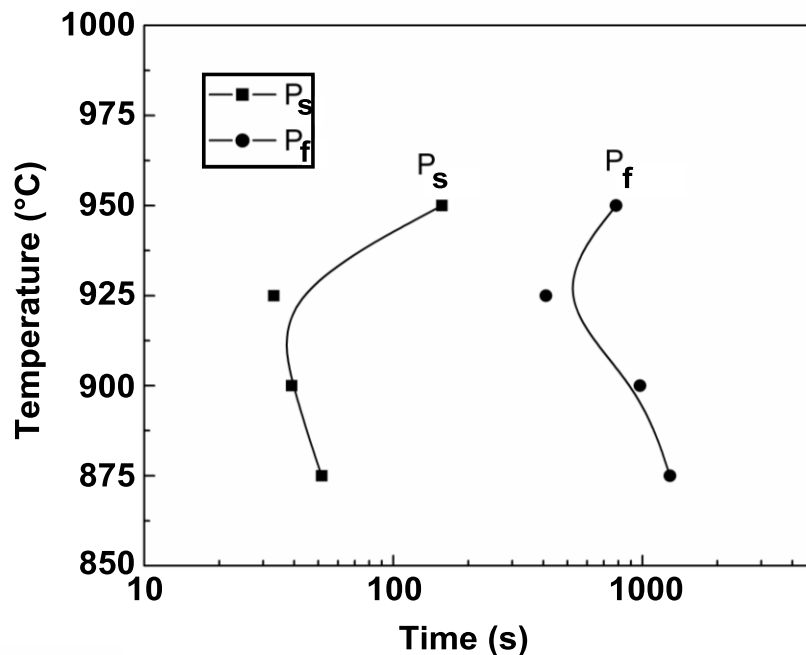


Figure 3. The PTT diagram of the studied Ti-Mo microalloyed steel, where P_s and P_f are the start and finish times of carbide precipitation, respectively.

Characterization of Precipitates in Ti-Mo Microalloyed Steel - Undissolved Precipitates

In the present work, a certain number of undissolved cube-shaped TiN particles, which could be formed during steelmaking and/or casting [17], were occasionally observed by TEM in the Ti-Mo microalloyed steel. As shown in Figure 4, these particles have a typical size of $\sim 1 \mu\text{m}$, so that they had little effect on the recovery and recrystallization of deformed austenite during stress relaxation [9,18]. Their number density was very small on the carbon replica film, which is due to the limited N content, 0.002 wt.%, in the studied alloy.

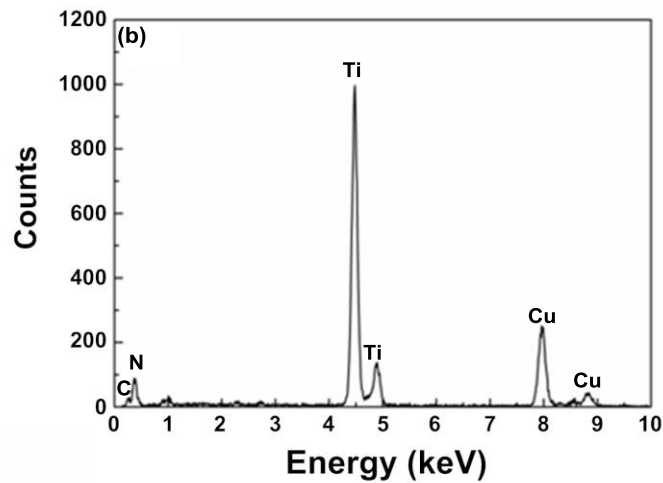
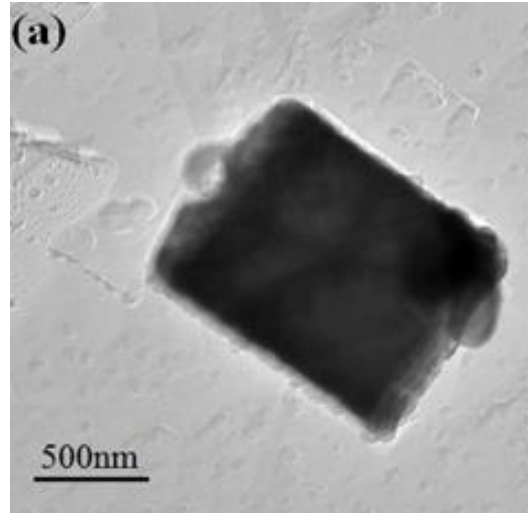


Figure 4. (a) TEM image showing an undissolved TiN particle in Ti-Mo microalloyed steel and (b) the corresponding EDS analysis of this TiN particle. It should be noted that the peaks of Cu on the EDS spectrum are from the Cu grid used to support the carbon replica film.

Precipitates Formed During Stress Relaxation in Ti-Mo Microalloyed Steel

Figure 5(a) is a TEM image showing a carbide particle formed in the specimen deformed at 925 °C followed by a hold for 1800 seconds, and it was identified as a Ti-rich MC carbide type with the NaCl-type crystal structure, containing a certain amount of Mo, by selected area electron diffraction (SAD) and EDS analysis as shown in Figures 5(b) and (c). The atomic ratio of Ti/Mo, quantified by EDS, in the carbide is about 8.0, which is larger than that of the (Ti,Mo)C particles in ferrite reported by Jang et al. [8] and Funakawa et al [1].

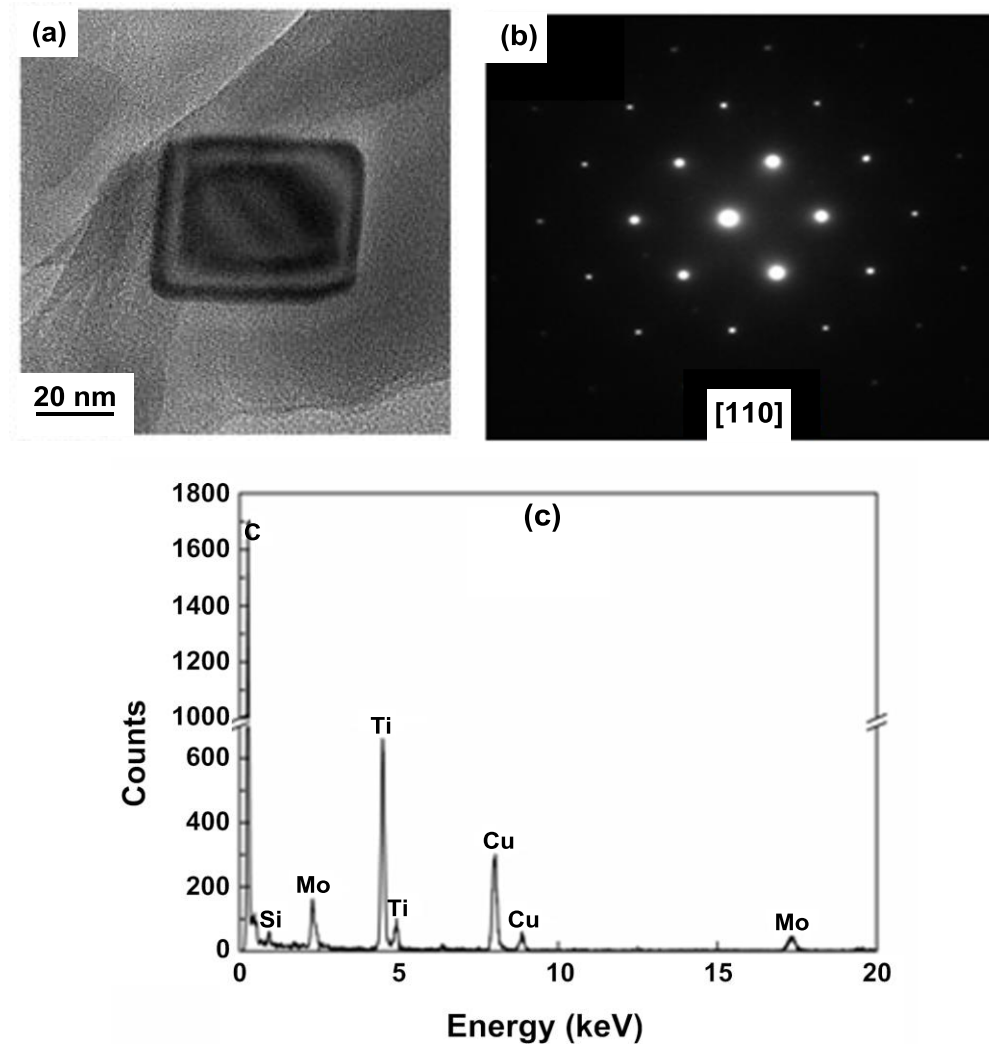


Figure 5. (a) TEM image showing a (Ti,Mo)C precipitate, (b) selected area electron diffraction (SAD) and (c) energy dispersive spectroscopy (EDS). It should be noted that the peaks of Cu and Si on the EDS spectrum are from the Cu grid used to support the carbon replica film and an inclusion on the carbon replica film, respectively.

The nucleation sites of the precipitates formed in the Ti-Mo microalloyed steel during stress relaxation can be confirmed indirectly by analyzing the distribution of particles on the carbon replica film. A high-angle annular dark-field scanning transmission electron microscopy (HAADF-STEM) image, shown in Figure 6, clearly exhibited a cell-like distribution of precipitates on the carbon replica, implying that the precipitates nucleated on dislocations or on dislocation sub-structures [13]. The sizes of these “sub-grains”, which were produced during deformation and a subsequent recovery process, were measured to be in the range of 0.2-1.0 μm , which is much smaller than the prior austenite grain size of $\sim 100 \mu\text{m}$.

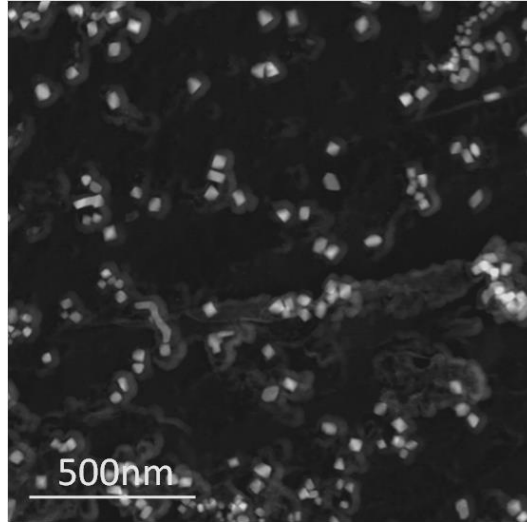


Figure 6. HAADF-STEM image showing the cell-like distribution of (Ti,Mo) carbides on carbon replica film, formed in the specimen deformed at 900 °C and held for 1800 seconds.

In addition, the shape of most of the precipitates, as seen in Figure 6, is polyhedral rather than a cube which had been identified from the TEM image in Figure 5. A precipitate which looked like a cube observed from a TEM image was selected as an example to clarify the difference. Figure 7 shows the TEM image (Figure 7(a)), STEM image of the precipitate (Figure 7(b)) and the corresponding selected area electron diffraction pattern (SAD) with a magnetic rotation angle of 90° relative to the TEM and STEM images (Figure 7(c)). It can be seen that the precipitate seems to have an almost perfect cube-like shape as shown in Figure 7(a). However, the strong three-dimensional contrast in Figure 7(b) together with the annular equal thickness fringes in Figure 7(a) indicate that the precipitate has a pyramid-like shape or an octahedral shape if the precipitate has a symmetry with respect to the observation plane, rather than a cube-like shape. Moreover, the two diagonals of this pyramid-like or octahedron-shaped precipitate were determined to be parallel with plane {200} of the precipitate, indicating that the majority of the facets were not on plane {200}. But the facet of the cube-like TiN particle precipitated in austenite is just in the plane {200} [19]. The equilibrium shape of M(C,N) particles with B1 structure, where M=Ti, Nb, V, Mo or their combination, depends on the interplay between interfacial and elastic strain energy minimization during precipitation in austenite [20]. According to Yang and Enomoto [19], the interfacial energy includes structure energy arising out of the lattice misfit between M(C,N) and the austenite matrix, and chemical energy from the difference in chemical composition at the M(C,N)/austenite interface. The elastic strain energy comes from the difference in elastic properties between M(C,N) and austenite. Yang and Enomoto [19] stated that the cube shape of TiN particles that adopt a cube-on-cube orientation relationship with respect to the austenite matrix, was mainly attributed to the anisotropy of the chemical interfacial energy, because the anisotropy of the structural interfacial energy of TiN/austenite interfaces (~15%) and the elastic strain energy are not large at higher temperatures. However, for other B1-carbides (and nitrides), ie. NbC, having a larger misfit with austenite (~22%) and considerable elastic strain energy due to its lower precipitation temperature, the cube-on-cube orientation relationship with respect to the austenite matrix may not always be maintained. Thus, the precipitate morphology is expected to become more irregular (see reference [21,22]). In the present study, the misfit between carbide and austenite was determined

as ~18% (lattice parameter equals ~0.43 nm) by SAD and assuming that the austenite lattice parameter is 0.365 nm [9]. This value lies in between that of TiN and NbC. Moreover, the precipitation temperature of the carbide in the present work is close to that of NbC reported in references [21,22], so that the elastic strain energy cannot be ignored under this condition. Therefore, the carbide in the present study is expected to exhibit a shape that lies in between that of TiN and NbC. Of course, accurately predicting the morphology of this carbide needs more work, including calculating interfacial energy, elastic strain energy and their particle size dependences, etc. However, this is beyond the scope of the present work.

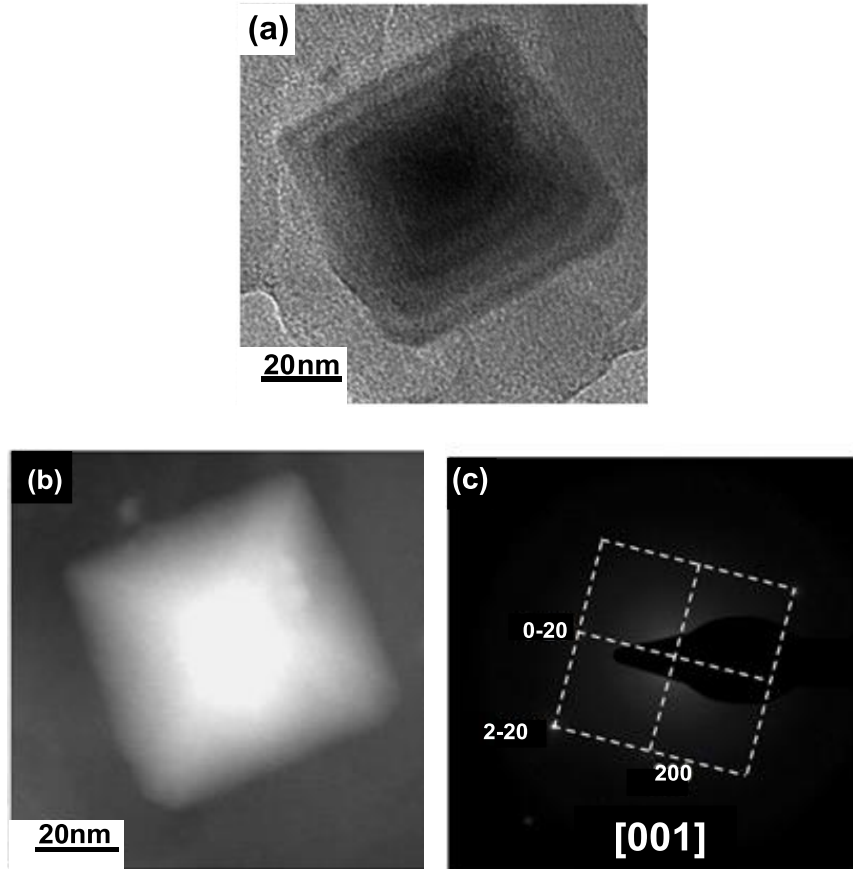


Figure 7. A carbide particle formed in the specimen deformed at 925 °C and held for 1800 seconds; (a) TEM image, (b) HAADF-STEM image and (c) the corresponding selected area electron diffraction (SAD). It should be noted that the shape of this precipitate is a rectangular pyramid or an octahedron as observed in (b) rather than a cube as seen in (a). In addition, the two diagonals of this pyramid or octahedral-shaped precipitate are on plane {200}, which is identified by SAD in (c).

A high-resolution transmission electron microscopy (HRTEM) investigation of the carbides formed in the Ti-Mo microalloyed steel was performed in this study, and an example of the lattice image of a carbide is presented in Figure 8(a). It was identified as a (Ti,Mo)C particle with a NaCl-type crystal structure using a two-dimensional fast Fourier transformation (FFT) analysis, which is consistent with the SAD result (see Figure 5). The lattice image obtained by an inverse fast Fourier transformation (IFFT) as shown in Figure 8(b) has been identified to have a lattice parameter of 0.43 nm, which is very close to that (0.423-0.430 nm) of the inter-phase precipitated (Ti,Mo)C particles reported by Yen et al. [7] and Funakawa et al. [1].

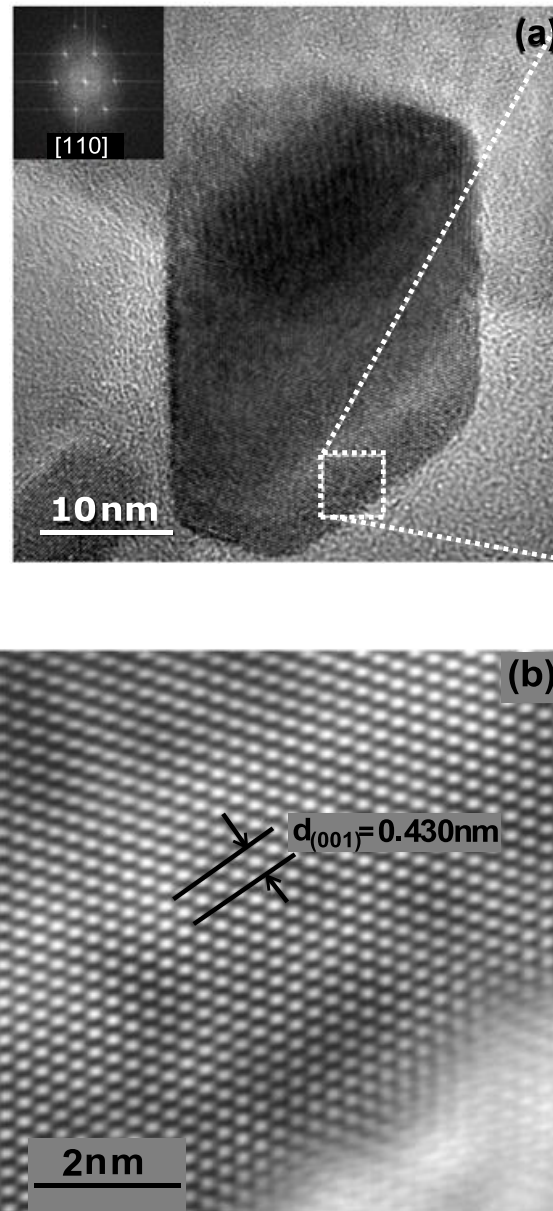
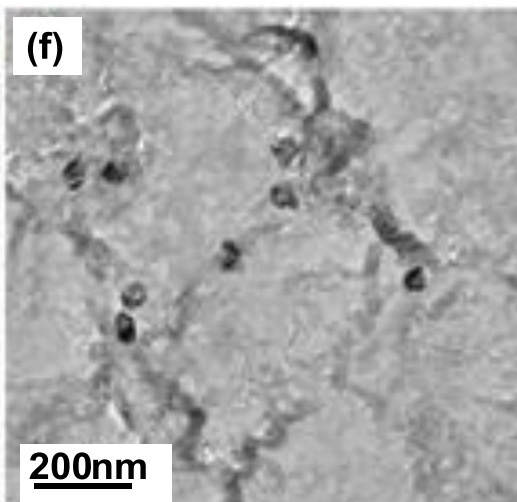
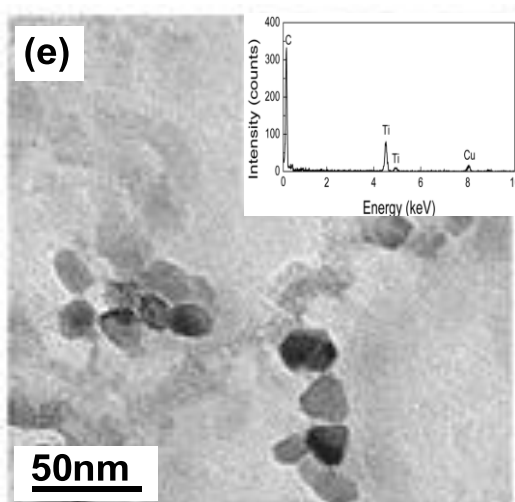
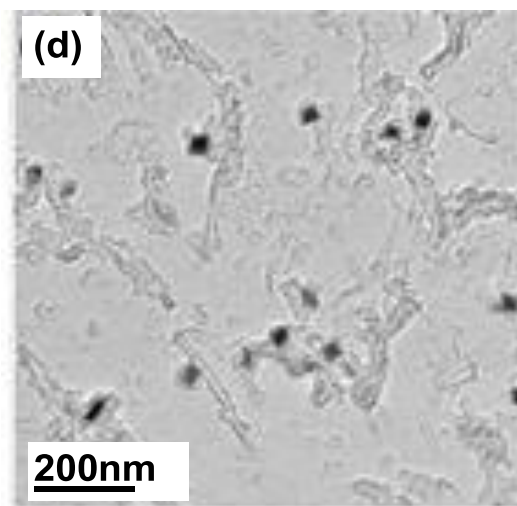
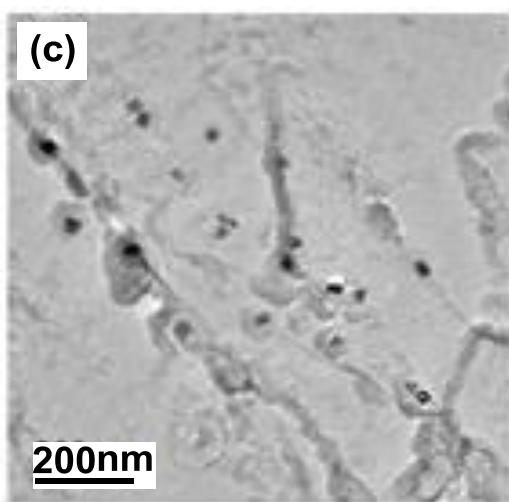
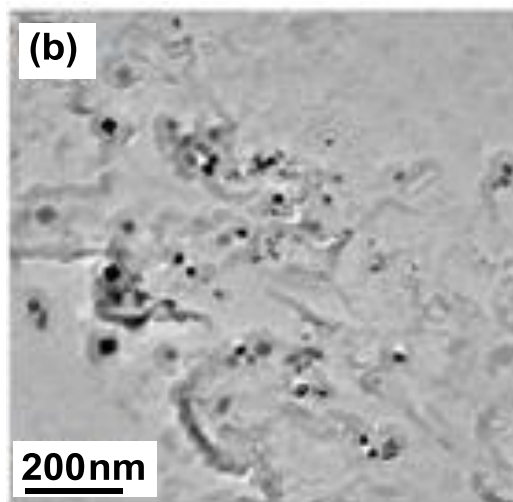
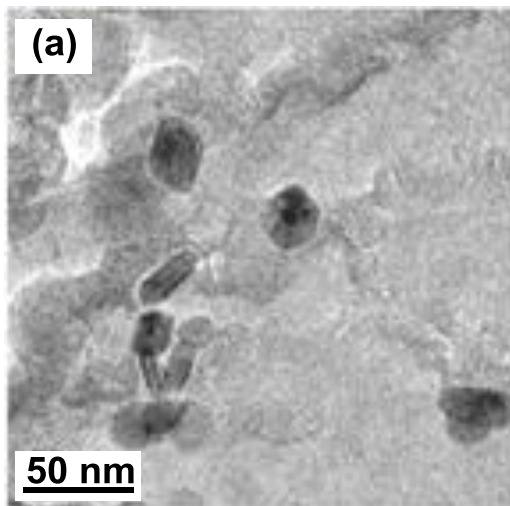


Figure 8. (a) HRTEM image showing a carbide particle in the specimen deformed at 925 °C and held for 3000 seconds and (b) IFFT lattice image of the area marked by a white-line frame on the carbide particle in (a).

Growth and Coarsening of Precipitates

In the present work, the particle size evolution of (Ti,Mo)C particles in the Ti-Mo microalloyed steel and TiC in the reference Ti steel, as a function of isothermal holding time, were investigated, and the results at the testing temperature of 925 °C are presented in Figure 9. It can be clearly seen that the carbide sizes in both steels were very close to each other for a 200 seconds holding time (see Figures 9(a) and (e)). However, with an increase of holding time to 600 seconds, to 1800 seconds and to 3000 seconds, (Ti,Mo)C particles in the Ti-Mo steel exhibited a smaller size and higher density than TiC in the Ti steel (see Figure 9(b), (c), (d), (f), (g) and (h)). In order to better understand the growth and coarsening behavior of carbides in the two steels, the average particle sizes for various holding times at 925 °C were measured and plotted in Figure 10. During the initial stage of precipitation, the carbides in both steels grow very quickly, and show almost the same growth rate. The growth of carbides at this stage approximately followed a parabolic law, ie. $d = \alpha\sqrt{Dt}$, where d is the size of the particle, α is the growth coefficient and D is the diffusion coefficient of the element which controls the growth rate. With an increase of holding time, the growth rate of the carbides slowed down in both steels, especially for the (Ti,Mo)C particles in the Ti-Mo steel, the average particle size being almost unchanged from 200 seconds to 1800 seconds. During this stage, precipitate development lies in the coarsening stage, ie. Ostwald ripening. The transition time from growth to coarsening was ~200 seconds for (Ti,Mo)C particles and ~600 seconds for TiC. It should be noted that the transition time from growth to coarsening for (Ti,Mo)C particles is roughly comparable with the P_f time (~400 seconds) given in the stress relaxation curve (see Figure 1). More importantly, (Ti,Mo)C particles in the Ti-Mo steel exhibit a superior coarsening resistance compared to TiC particles in the Ti steel during this stage, as shown in Figure 10. This phenomenon has often been observed [1,5,6-8] for (Ti,Mo)C particles precipitated in ferrite or during the $\gamma \rightarrow \alpha$ phase transformation.



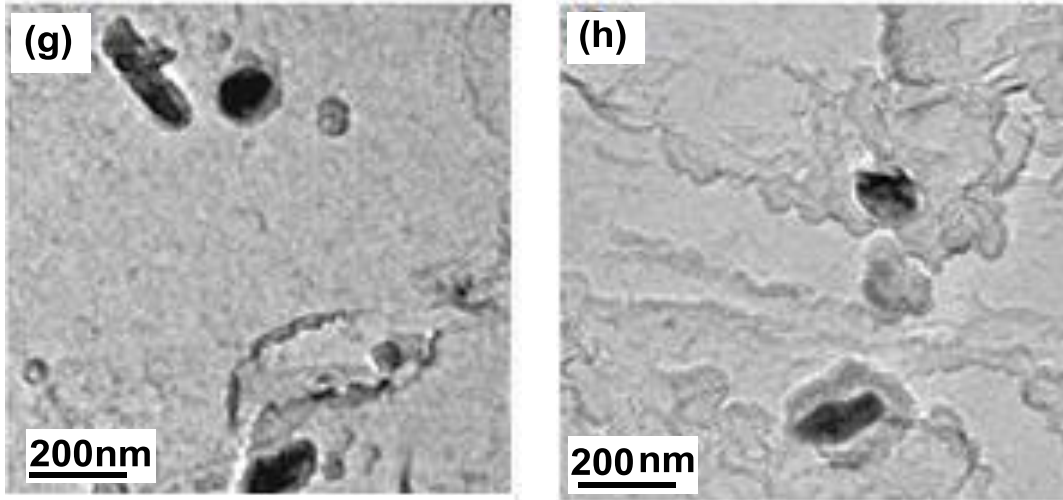


Figure 9. (a)-(d) TEM images showing carbide particles formed at 925 °C for various holding times in Ti-Mo microalloyed steel; (a) 200 seconds, (b) 600 seconds, (c) 1800 seconds and (d) 3000 seconds. (e)-(h) TEM images showing carbide particles formed at 925 °C for various holding times in Ti microalloyed steel; (e) 200 seconds, (f) 600 seconds, (g) 1800 seconds and (h) 3000 seconds.

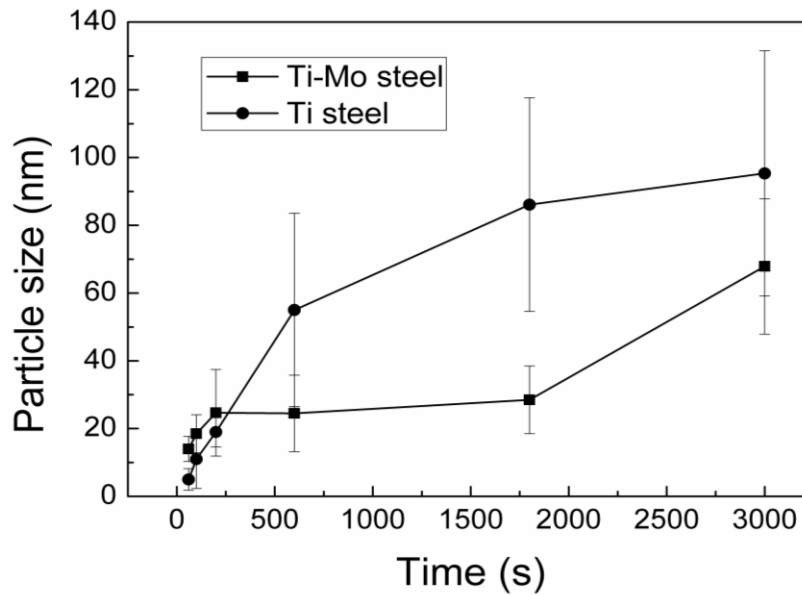


Figure 10. Average particle sizes of carbides at 925 °C as a function of isothermal holding time.

The relationship between average particle size and holding time during the initial stage of precipitation, before 200 seconds, for the Ti-Mo steel and before 600 seconds for the Ti steel, is roughly determined as $d = kt^{\frac{1}{2}}$, where d is the average size of the particle, k is a constant and t is the isothermal holding time.

According to Ostwald's ripening theory:

$$d_t^n - d_0^n = \frac{k}{RT} V_m^2 CD\gamma t \quad (3)$$

where d_t is average particle size at a given time, d_0 is the initial average particle size, n is 3 for volume diffusion controlled coarsening, k is a constant, V_m is the molar volume of the precipitate, C is the concentration of solute in the matrix that is in equilibrium with the precipitate, D is the diffusivity of the solute, γ is the interfacial energy per unit area between the precipitate and the matrix, R is the gas constant and T is the absolute temperature. The coarsening rate of a carbide at a given temperature T is mainly dependent on the interfacial energy γ , the diffusivity D and the concentration C of the rate controlling element in austenite [8,9].

Since interstitial atoms diffuse much faster than substitutional atoms in austenite, the coarsening process is considered to be controlled by the diffusion of substitutional elements Ti or Mo. According to Yong's theory [9], the coarsening process of ternary (Ti,Mo)C particles depends on the product of D and C of substitutional solute atoms in austenite. The element that has a smaller product of D and C is considered as the controlling element. As discussed in a previous section, (Ti,Mo)C particles are rich in Ti rather than Mo, so that the concentration of Ti in solution is much lower than that of Mo during the coarsening stage. In addition, the diffusivity of Ti in austenite is a little larger (~1.1-1.2 times) than that of Mo over the investigated temperature range [9]. Therefore, on balance, the controlling element in the coarsening process of (Ti,Mo) carbides in the Ti-Mo steel is determined as Ti, which is also the controlling element for the TiC coarsening process in the Ti steel. In another work that will be published [23], the effect of Mo on the kinetics of carbide precipitation in Ti microalloyed steel was investigated by hot rolling experiments. Figure 11 is the physical-chemical phase analysis result showing the precipitated amount of Ti in carbide (TiC or (Ti,Mo)C) for 600 seconds and 1800 seconds isothermal holding at ~925 °C in Ti and Ti-Mo steels. The results show that the addition of Mo into a Ti steel can increase the amount of Ti precipitated as carbide from the austenite. Therefore, the remaining Ti solute in austenite for the Ti-Mo steel is lower than for the Ti steel during the coarsening process. Consequently, the decreased Ti concentration caused by the Mo addition is considered to result in the decrease of the coarsening rate of (Ti,Mo)C particles according to Equation (3). On the other hand, the lattice parameters of carbides were identified by TEM/SAD as ~0.430 nm for both (Ti,Mo)C and TiC. Therefore, the lattice misfit between carbide and austenite matrix is almost the same for the two steels, indicating that the structural interfacial energy of (Ti,Mo)C particles approximately equals that of TiC particles if the cube-on-cube orientation relationship is maintained between the carbide and austenite [9]. However, the partial replacement of Ti by Mo in the TiC crystal lattice results in a decrease of the contributions of chemical binding to the interfacial energy of carbide/austenite according to our calculation result [23] and Yang's DLP/NNBB theory [24,25]. Thus, the chemical interfacial energy is possibly reduced by the partial replacement of Ti by Mo in the TiC lattice, although the exact chemical interfacial energy depends on the spread over which the interface is defined. As a result, the total interfacial energy of a (Ti,Mo)C particle with austenite is possibly reduced as compared with that of TiC, and this in turn decreases the coarsening rate of (Ti,Mo) carbides according to Equation (3).

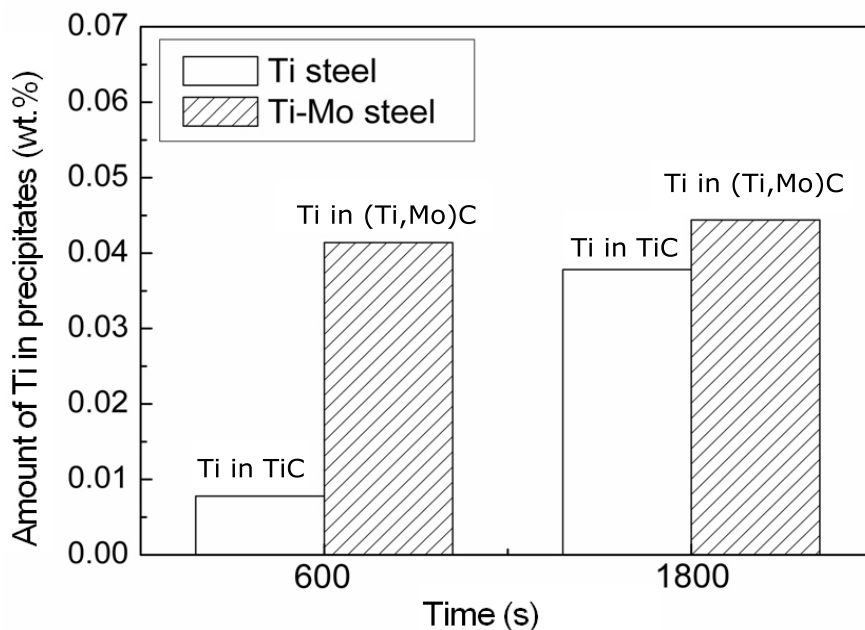


Figure 11. Physical-chemical phase analysis showing the precipitated amount of Ti in carbide (TiC or (Ti,Mo)C) for 600 seconds and 1800 seconds isothermal holding time after one pass rolling with a reduction of 20% at ~ 925 °C in Ti and Ti-Mo microalloyed steels. It should be noted that the total Ti content is 0.1 wt.% for both steels [23].

Thermodynamic and Kinetic Analysis for (Ti,Mo)C Phase

In this paper, the compositional evolution of (Ti,Mo)C particles in a Ti-Mo steel was studied at the testing temperature of 925 °C. As shown in Figure 12, the atomic ratio of Ti/Mo in (Ti,Mo)C particles increased with isothermal holding time or particle growth. This phenomenon seems to indicate that, on the one hand, the incorporation of Mo into TiC favors the nucleation and growth during the early stages of precipitation, but on the other hand, the high level of Ti replacement by Mo in the TiC lattice is “metastable” with respect to equilibrium precipitation of (Ti,Mo)C phase. Figure 13 shows the variations of the equilibrium atomic fractions of Ti, Mo and C in MC phase, with temperature, calculated by Thermo-calc, (Figure 13(a) – Ti, Figure 13(b) – Mo, Figure 13(c) – C). FCC and BCC phases were selected for the Thermo-calc calculations. This meant that the MC phase was in equilibrium with austenite at higher temperatures and with ferrite at lower temperatures. In addition, the calculated MC phase contained a small amount of Fe and Mn, thus leading to the sum of atom fractions of Ti and Mo not being 0.5 as shown in Figures 13(a) and (b), especially at lower temperatures. In Figure 13, the equilibrium chemical composition of the MC phase with FCC structure approaches pure TiC at temperatures above 800 °C. As the temperature decreases, the equilibrium atomic fraction of Mo in the MC phase increases. When the temperature decreases to below 700 °C, the rate of increase of the atomic fraction of Mo with temperature becomes larger. The atomic ratio of Mo/Ti is about 1.0 in the temperature range of 500-600 °C. The measured atomic fractions of Mo by EDS in MC phase at different temperatures for 1800 seconds isothermal holding time are also shown (black circles) in Figure 13(b). Here, it is assumed that no vacancies are present at C atom positions in the MC lattice, namely a perfect NaCl-type MC phase. In this case, the atomic fraction of Mo in MC reaches the minimum

because the partial replacement of Ti by Mo in the TiC lattice possibly produces a certain amount of vacancies at C atom positions according to reference [8]. In addition, the experimental result (shown as black diamond) from Funakawa et al [1], for a Ti-Mo microalloyed steel with a similar chemical composition to that of the present steel was given in Figure 13(b) for comparison, (specimen held at 620 °C for 3600 seconds after finish rolling and furnace cooled to room temperature) As the temperature decreases, the measured atomic fraction of Mo in MC phase increases. However, the values are much higher than those calculated by Thermo-calc, and the difference becomes larger with decreasing temperature, for example, ~3% at 950 °C, but up to ~8% at 875 °C. The steel from Funakawa et al, showed a difference of ~11%. As discussed above, the site fraction of Mo in the (Ti,Mo)C lattice decreases with isothermal holding time or with particle growth. Such a finding, together with the comparison between the experimental results and theoretical calculations, indicates that the greater replacement of Ti by Mo in the TiC lattice is energetically unfavorable with respect to the equilibrium precipitation, when the other energy conditions, including interfacial energy and elastic strain energy, between precipitate and matrix are not considered.

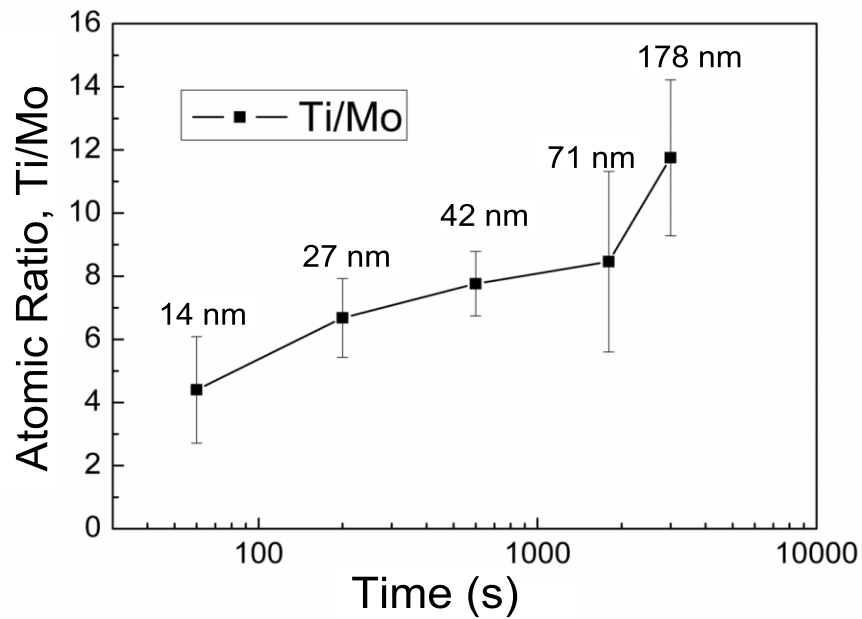
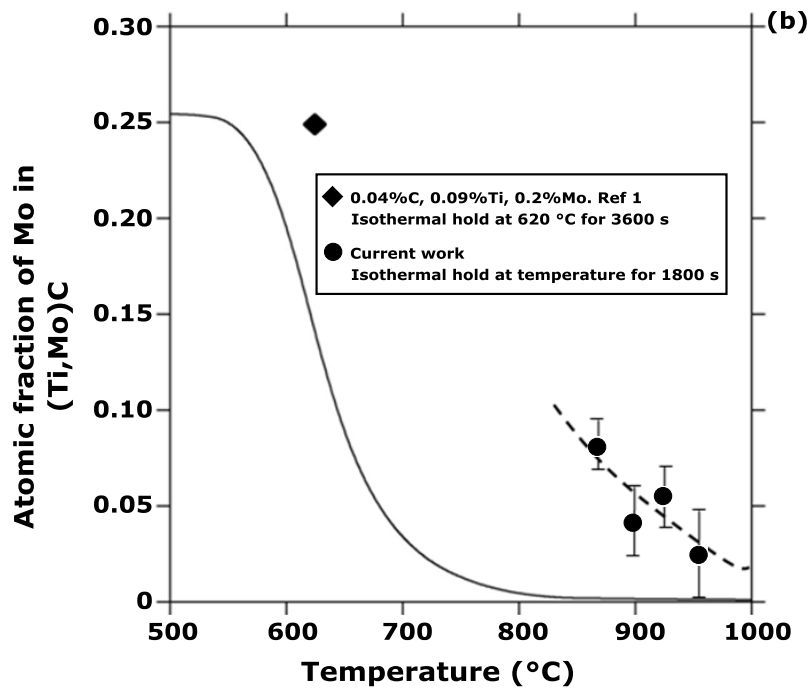
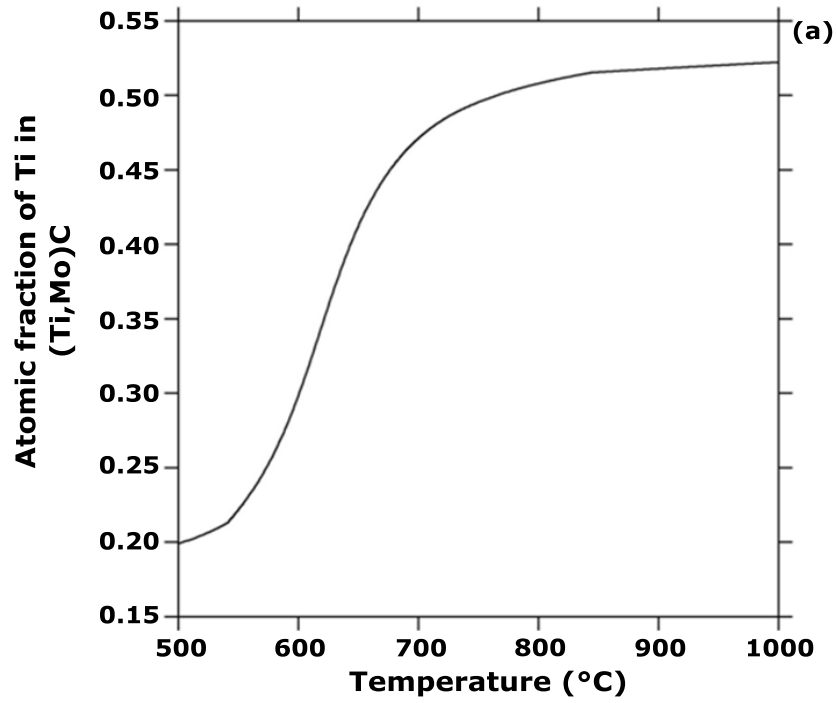


Figure 12. Atomic ratio of Ti/Mo in carbide as a function of isothermal holding time at 925 °C. The figures above the Ti/Mo- $\log(\text{time})$ curve represent the average particle sizes of the measured precipitates.



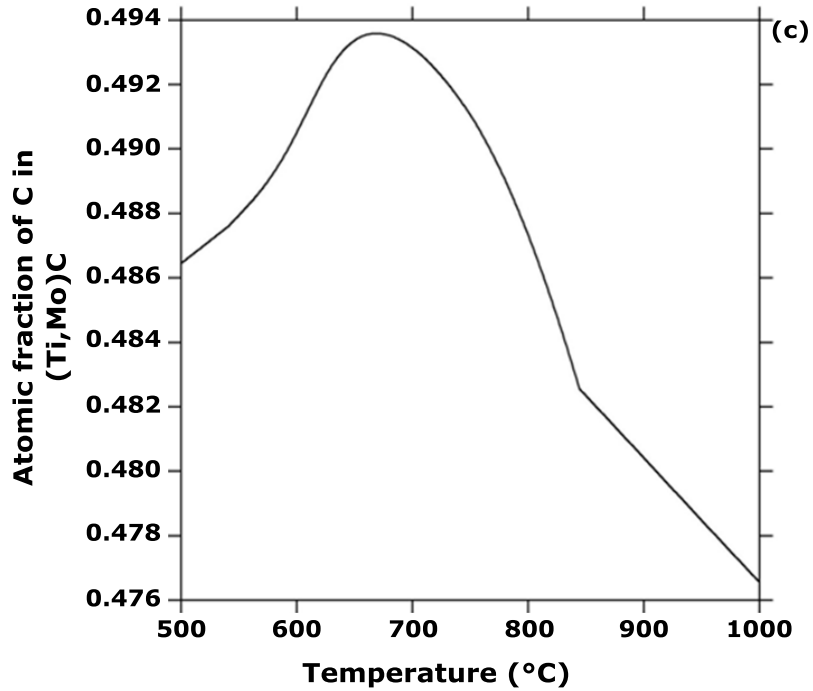


Figure 13. Variations of equilibrium atomic fractions of; (a) Ti, (b) Mo and (c) C in MC carbide particle with temperature as calculated using Thermo-calc with database TCFE6. (The datapoints shown as black circles in Figure 13(b) are from the current work for an isothermal hold of 1800 s).

As discussed in a previous section, the partial replacement of Ti by Mo in the TiC lattice possibly decreases the chemical interfacial energy between (Ti,Mo)C and austenite [23]. Therefore, this effect, in fact, favors the decrease of the nucleation energy barrier, thus enhancing the nucleation of (Ti,Mo)C phase during the early stages of precipitation. Accordingly, smaller (Ti,Mo)C particles contain more Mo as shown in Figure 12. However, with particle growth, the surface area to volume ratio of the particle becomes less significant, i.e. the interface effect becomes not so significant. Thereupon, the incorporation of Ti into (Ti,Mo)C phase becomes more beneficial to the decrease of the total free energy of the system, thus resulting in the decrease of the fraction of Mo in the (Ti,Mo)C phase, as shown in Figure 12. However, the incorporation rate of Ti atoms into (Ti,Mo)C phase depends on the diffusivity of Ti in austenite, which is a function of isothermal temperature. The diffusion rate of Ti atoms is slower at lower temperatures, thus leading to the larger difference, in terms of the fraction of Mo in (Ti,Mo)C phase, between the experimental measurements and the equilibrium results calculated by Thermo-calc at lower temperatures.

Conclusions

The precipitation-time-temperature diagram for the kinetics of carbide precipitation in Ti-Mo microalloyed steel determined by a stress relaxation method exhibited a typical “C” shape curve, and its nose was located at ~925 °C. The precipitates formed during stress relaxation in the Ti-Mo microalloyed steel were identified as polyhedral Ti-rich (Ti,Mo) carbides possessing a NaCl-type crystal structure that contains a certain amount of Mo. The (Ti,Mo)C precipitates were heterogeneously distributed in a cell-like manner, implying that the precipitates nucleated on dislocations or on dislocation sub-structures, which were produced by deformation. The growth of carbide particles in the Ti-Mo microalloyed steel approximately followed a parabolic law during the growth stage. During the coarsening stage, (Ti,Mo)C particles in the Ti-Mo microalloyed steel exhibited a higher coarsening resistance as compared with TiC particles in the Ti microalloyed steel, which is attributed, on the one hand, to the decrease of Ti concentration in austenite by the accelerating effect of Mo on Ti precipitation as carbide and, on the other hand, possibly to the decrease in the chemical interfacial energy of carbide/austenite by the incorporation of Mo into the TiC lattice.

References

1. Y. Funakawa et al., “Development of High Strength Hot Rolled Sheet Consisting of Ferrite and Nanometer-sized Carbides,” *The Iron and Steel Institute of Japan International*, 44 (2004), 1945-1951.
2. T. Shimizu, Y. Funakawa and S. Kaneko, “High Strength Steel Sheets for Automobile Suspension and Chassis Use – High Strength Hot Rolled Steel Sheets with Excellent Press Formability and Durability for Critical Safety Parts,” *JFE Technical Report*, 4 (2004), 25-31.
3. K. Yamada, K. Sato and H. Nakamichi, “Analysis of Nanometer-sized Precipitates using Advanced TEM,” *JFE Technical Report*, 9 (2007), 5-11.
4. M. Nagoshi, T. Kawano and K. Sato, “Quantitative Chemical State Analysis of Ti and Mo in a High Strength Steel Using X Ray Absorption Fine Structure (XAFS),” *JFE Technical Report*, 9 (2007), 12-15.
5. Y. Funakawa and K. Seto, “Coarsening Behavior of Nanometer-sized Carbides in Hot Rolled High Strength Sheet Steel,” *Materials Science Forum*, 539 (2007) 4813-4818.
6. C.Y. Chen et al., “Precipitation Hardening of High Strength Low Alloy Steels by Nanometer-sized Carbides,” *Materials Science and Engineering A*, 499 (2009) 162-166.
7. H.W. Yen, C.Y. Huang and J.R. Yang, “Characterisation of Interphase Precipitated Nanometer-sized Carbides in a Ti-Mo Bearing Sheet,” *Scripta Materialia*, 61 (2009), 616-619.
8. J.H. Jang et al., “Stability of (Ti,M)C (M=Nb,V,Mo and W) Carbide in Steels using First Principles Calculations,” *Acta Materialia*, 60 (2012), 208-217.

9. Q.L. Yong, Secondary Phases in Steels. Metall Industry Press, Beijing (2006).
10. H.S. Zurob et al., "Modelling Recrystallisation of Microalloyed Austenite: Effect of Coupling Recovery, Recrystallisation and Precipitation," *Acta Materialia*, 50 (2002), 3075-3092.
11. B. Dutta, E.J. Palmiere and C.M. Sellars, "Modelling the Kinetics of Strain Induced Precipitation in Nb Microalloyed Steels," *Acta Materialia*, 49 (2001), 785-794.
12. W.J. Liu and J.J. Jonas, "A Strain Relaxation Method for Following Carbonitride Precipitation in Austenite at Hot Working Temperatures," *Metallurgical Transactions*, 19A (1988), 1403-1413.
13. Z.Q. Wang et al., "Strain Induced Precipitation in a Ti Microalloyed HSLA Steel," *Materials Science and Engineering A*, 529 (2011), 459-467.
14. M.G. Akben et al., "Dynamic Precipitation and Solute Hardening in a Titanium Microalloyed Steel Containing Three Levels of Manganese," *Acta Metallurgica*, 32 (1984), 591-601.
15. A. Pandit et al., "Strain Induced Precipitation of Complex Carbonitrides in Nb-V and Ti-V Microalloyed Steels," *Scripta Materialia*, 53 (2005), 1309-1314.
16. W.J. Liu and J.J. Jonas, "Ti(CN) Precipitation in Microalloyed Austenite During Stress Relaxation," *Metallurgical Transactions*, 19A (1988), 1415-1424.
17. X.P. Mao et al., *Acta Metallurgica Sinica*, 42 (2006), 1091-1095. (In Chinese)
18. J. Moon and C.H. Lee, "Pinning Efficiency of Austenite Grain Boundary by a Cubic Shaped TiN Particle in Hot Rolled HSLA Steel," *Materials Characterization*, 73 (2012), 31-36.
19. M. Enomoto and Z.G. Yang, "Calculation of the Equilibrium Shape of TiN Particles in Iron," *The Iron and Steel Institute of Japan International*, 44 (2004), 1454-1456.
20. R. Shi, N. Ma and Y. Wang, "Predicting Equilibrium Shape of Precipitates as Function of Coherency State," *Acta Materialia*, 60 (2012), 4172-4184.
21. S.G. Hong, K.B. Kang and C.G. Park, "Strain Induced Precipitation of NbC in Nb and Nb-Ti Microalloyed HSLA Steel," *Scripta Materialia*, 46 (2002), 163-168.
22. J.S. Park, Y.S. Ha and Y.K. Lee, "Comparison of Experimental Methods to Measure the Isothermal Precipitation Kinetics of Nb(C,N) in Austenite of a Nb Microalloyed Steel," *Metallurgical and Materials Transactions*, 40 A (2009), 1515-1519.
23. Z.Q. Wang et al., "Effect of Mo Addition on the Kinetics of Carbide Precipitation in Ti Microalloyed Steel. (unpublished work)

24. Z.G. Yang and M. Enomoto, "A Discrete Lattice Plane Analysis of Coherent FCC/B1 Interfacial Energy," *Acta Materialia*, 47 (1999), 4515-4524.

25. Z.G. Yang and M. Enomoto, "Calculation of the Interfacial Energy of B1-type Carbides and Nitrides with Austenite," *Metallurgical and Materials Transactions*, 32 A (2001), 267-274.